Geophysical Research Letters

RESEARCH LETTER
10.1029/2026GL123087

Evolution of NWC Transmitter Wave Power Distribution From the Topside Ionosphere Into the Inner Magnetosphere

Zhiyang Xia[1], Lunjin Chen[1], Richard B. Horne[2], Yoshizumi Miyoshi[3], Yoshiya Kasahara[4], Shoya Matsuda[4], Atsuki Shinbori[3], Tomoaki Hori[3], and Iku Shinohara[5]

[1]Department of Physics, University of Texas at Dallas, Richardson, TX, USA, [2]British Antarctic Survey, Cambridge, UK, [3]Institute for Space-Earth Environmental Research, Nagoya University, Nagoya, Japan, [4]Graduate School of Natural Science and Technology, Kanazawa University, Kanazawa, Japan, [5]Institute of Space and Astronautical Science, Japan Aerospace Exploration Agency, Sagamihara, Japan

Key Points:

- The observed North West Cape wave power from Van Allen Probes and Energization and Radiation in Geospace/Arase shows a concentric rings pattern in the magnetosphere, like the ionosphere
- As transmitter signals propagate further away from the transmitter, the concentric rings pattern becomes less distinct and moves outward
- The non-ducted propagation with spread initial wave normal angles can account for the evolution of the wave power distribution

Supporting Information:

Supporting Information may be found in the online version of this article.

Correspondence to:

Z. Xia,
zhiyang.xia@utdallas.edu

Citation:

Xia, Z., Chen, L., Horne, R. B., Miyoshi, Y., Kasahara, Y., Matsuda, S., et al. (2026). Evolution of NWC transmitter wave power distribution from the topside ionosphere into the inner magnetosphere. *Geophysical Research Letters*, *53*, e2026GL123087. https://doi.org/10.1029/2026GL123087

Received 18 MAR 2026
Accepted 23 MAY 2026

Abstract Ground-based very low frequency transmitters emit signals that primarily propagate within the Earth–ionosphere waveguide, and some of their energy can propagate into the magnetosphere. Ionospheric observations from the DEMETER satellite reveal a distinct concentric rings pattern of the wave power distribution of the North West Cape transmitter on the transverse (longitude–L-shell) plane. Using data from the Van Allen Probes and Arase/energization and Radiation in Geospace satellites, we find that the concentric rings pattern is still visible but becomes less distinct. The pattern shifts outward, and becomes more elliptic as the wave propagates from the southern ionosphere to the Northern Hemisphere. To investigate the cause of this evolution, we performed ray tracing simulations under three conditions: ducted propagation, non-ducted propagation with vertical initial wave normal angles and non-ducted propagation with spread initial wave normal angles. The results show that non-ducted propagation with spread wave normal angles best explains the observed evolution of wave power distribution pattern during the propagation.

Plain Language Summary Very low frequency (VLF) radio transmitters on the ground are mainly used for long-distance communication. Some of the transmitted wave energy can escape upward into near-Earth space and interact with energetic electrons in the inner magnetosphere. Previous research has mostly focused on how VLF wave power spreads on the meridional plane (over latitude and L-shell). In this study, we use data from the DEMETER, Van Allen Probes, and Energization and Radiation in Geospace/Arase satellites to examine how waves from the North West Cape transmitter are distributed on the transverse plane (over longitude and L-shell) and how this distribution evolves during propagation in the inner magnetosphere. The transverse distribution of wave power shows concentric ring-like patterns near the topside ionosphere, and this pattern moves outward and becomes less distinct as the waves propagate from the Southern Hemisphere to the Northern Hemisphere. By comparing with ray-tracing simulation results, we show that non-ducted propagation with broad initial wave normal angles primarily accounts for the observed changes in the wave power distribution.

1. Introduction

Ground-based very low frequency (VLF) transmitters are utilized primarily for long range communication. Most electromagnetic waves emitted by VLF transmitters propagate within the Earth–ionosphere waveguide (Budden, 1961); however, a portion of the wave power can leak upward into the ionosphere and subsequently propagate into the inner magnetosphere. As an important type of whistler-mode waves in the inner magnetosphere, VLF transmitter waves can cause the pitch angle scattering of the energetic electrons in the radiation belt through wave-particle resonance and drive the precipitation of electrons into the atmosphere (Chen et al., 2026; Claudepierre et al., 2020; Cunningham et al., 2020; Gamble et al., 2008; Graf et al., 2009; Inan et al., 2007; Kulkarni et al., 2008; Li et al., 2012; Liu et al., 2022; Ma et al., 2017; Rodger et al., 2010; Ross et al., 2019; Sauvaud et al., 2008; Selesnick et al., 2013; Shen et al., 2022).

Two theories of VLF transmitter wave propagation in the magnetosphere have been proposed: the ducted mode (Helliwell, 1966) and the non-ducted mode (Cerisier, 1973). The ducted mode requires the presence of density irregularities that confine the wave propagation along the background magnetic field line, whereas the non-ducted mode does not require such irregularities and can occur in a smoothly varying density profile. Different

propagation modes of VLF transmitter signals lead to distinct distributions of wave power and wave-normal angle in the inner magnetosphere, thereby influencing the loss processes of energetic electrons (Albert et al., 2020; Ma et al., 2022; Rodger et al., 2010). Observations from several inner magnetospheric spacecraft (e.g., Van Allen Probes, Cluster, ERG/Arase) have enabled studies of the wave-power distribution on the meridional plane of VLF transmitter emissions (Němec et al., 2025; Starks et al., 2020; Xia et al., 2023; Zhang et al., 2018). Numerical simulations, including ray-tracing and full-wave models, have also been used to reproduce transmitter-driven wave-power distributions (Němec et al., 2025; Starks et al., 2008, 2020). The propagation mode can be inferred by comparing in situ satellite observations with simulation results for different propagation scenarios. Moreover, burst-mode waveform measurements of multiple field components allow direct calculation of wave-normal angles and further analysis of propagation modes (Gu et al., 2020, 2021; Němec et al., 2022). However, most previous studies have focused on wave-power distributions on the meridional plane (over latitude and L-shell). How VLF transmitter wave power is distributed on the transverse plane (over longitude and L-shell), as well as how this distribution evolves during propagation in the inner magnetosphere, remains insufficiently investigated.

In this study, by combining observations from DEMETER, the Van Allen Probes, and ERG/Arase, we systematically analyze the wave power distribution on the transverse plane of the North West Cape (NWC) transmitter, and compare the distributions at different latitudes in the inner magnetosphere. The NWC transmitter is located at NWC (geomagnetic latitude of −31.96° and longitude of 186.4°), Western Australia, with an operating frequency of 19.8 kHz and very strong power of approximately 1 MW. The observed wave power distribution on the transverse plane is compared with the ray tracing simulation results to investigate the main propagation mode accounting for the evolution of the wave power distribution. Section 2 provides a brief description of the spacecrafts and instruments for the observational data used in this study. Section 3 analyzes the observed wave power distribution and the corresponding evolution in the inner magnetosphere. Section 4 uses a ray tracing simulation to verify and explain the observed evolution of the wave power distribution.

2. Spacecraft and Instruments

DEMETER (Detection of Electro-Magnetic Emissions Transmitted from Earthquake Regions) was a French satellite operated over a ∼6.5-year period from June 2004 to December 2010. It had a low-altitude, nearly Sun-synchronous circular orbit (∼10:30 and ∼22:30 LT) with an altitude of initially 710 km before December 2005 and 660 km thereafter (Parrot et al., 2006). The Instrument Champ Electrique (Berthelier et al., 2006) onboard can provide measurements of the electric field with a frequency range from DC/ULF band (0–15 Hz) up to HF band (10 kHz–3.175 MHz). The data used in this study consist of single-component VLF-band electric field wave spectra measurements, with a time resolution of about 4 s, a frequency resolution of 19.53 Hz, and a frequency range from 19.53 Hz to 20 kHz.

The Van Allen Probes (Mauk et al., 2013) were twin satellites with identical instruments and nearly identical near-equatorial orbits with a perigee of approximately 1.1 Earth radius (R_E), an apogee of approximately 5.8 R_E, as well as an orbital period of about 537 min. The satellites were launched in August 2012, and the mission ended in October 2019, with an operating duration of approximately 7 years. The high-frequency receiver of the Electric and Magnetic Field Instrument Suite and Integrated Science (EMFISIS) (Kletzing et al., 2013) can provide the measurement of wave power spectra of one component of the wave electric field in the plane perpendicular to the spacecraft spin axis. The time resolution of the data product is 6 s, and the frequency range spans from 10 to 400 kHz.

The Exploration of energization and Radiation in Geospace (ERG) (Miyoshi, Shinohara, et al., 2018) satellite with the nickname "ARASE" was launched on 20 December 2016, with apogee and perigee of ∼32,000 and 460 km, respectively, and an orbital period of ∼570 min. The onboard frequency analyzer (Matsuda et al., 2018) of the measurements from the Plasma Wave Experiment (PWE) instrument (Kasahara, Kasaba, et al., 2018) measures the one component electric field in the plane perpendicular to the spacecraft spin axis from DC to 20 kHz at 1 s sampling with a fine Δf (0.064–0.832 kHz in a nominal operation mode). The inclination of ERG/Arase orbits (∼31°) is higher than that of the Van Allen Probes, which can provide middle latitude coverage of VLF transmitter emissions.

For the DEMETER satellite, measurements are binned into 360 geomagnetic longitude bins and 181 geomagnetic latitude bins, each with a resolution of 1°. The arithmetic mean of the electric field wave power is calculated for

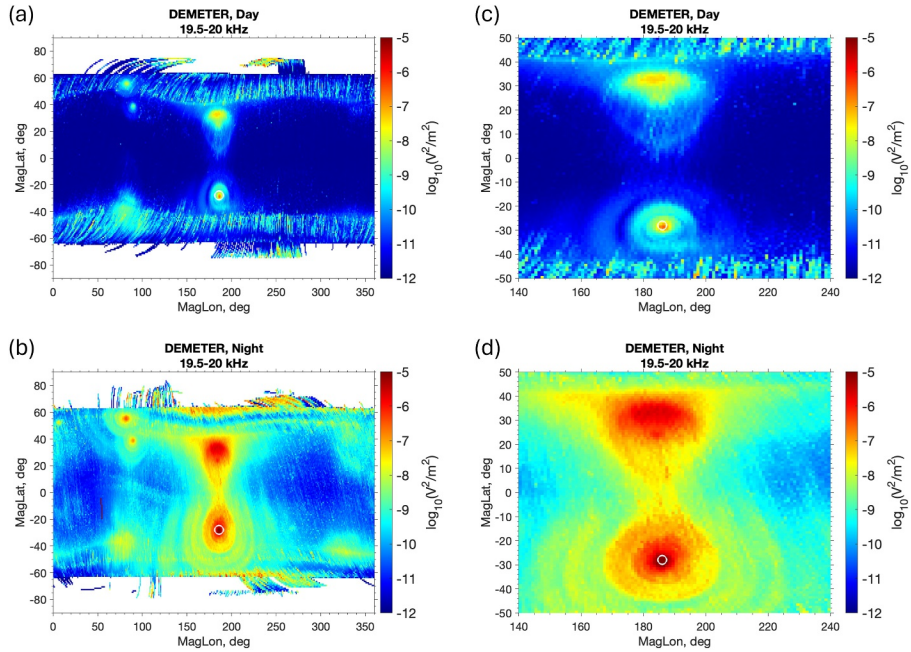

Figure 1. The mean electric field wave power distribution of North West Cape transmitter emission versus geomagnetic latitude and longitude at 700 km altitude observed by DEMETER satellite. (a) and (b) are global distributions for day and night sides, respectively. (c) and (d) are the zoom-in view of (a) and (b) around the location of NWC transmitter and its conjugate point.

each bin over the frequency range of 19.5–20 kHz. For the Van Allen Probes, satellite locations are traced to their 700 km ionospheric footprints using the International Geomagnetic Reference Field model (Thébault et al., 2015). Observations with positive (negative) local magnetic latitude are mapped to the Northern (Southern) Hemisphere. The mapped footprints are then binned using the same geomagnetic longitude and latitude grid as for DEMETER, and the arithmetic mean wave power is calculated for the 19.573 kHz frequency bin. ERG/Arase observations are processed following the same procedure as for the Van Allen Probes, except that the satellite locations, together with the associated observations, are mapped to footprints of 100 km altitude in both hemispheres. In addition, the data are categorized into three local magnetic latitude ranges: $\leq -15°$, $-15°$ to $15°$ and $\geq 15°$.

3. In-Situ Spacecraft Observation

Figure 1 shows the distribution of mean electric field wave power of NWC transmitter (19.5–20 kHz) over geomagnetic longitude and latitude at about 700 km altitude observed by DEMETER satellite. Figures 1a and 1b are the day side and night side observations, and Figures 1c and 1d are the corresponding zoom-in views in the region around NWC transmitter and its conjugate point, respectively. Intense wave power can be observed around the location of NWC transmitter in the Southern Hemisphere and its conjugate point in the Northern Hemisphere. The maximum wave power is near latitude of $-28°$ and longitude of $186°$ (labeled by the white circles), which is close to the location of NWC transmitter (latitude of $-31.96°$ and longitude of $186.4°$). The wave power on the night side is stronger than the day side since the wave damping during the propagation from the ground to the ionosphere is much weaker on the night side. Several clear concentric rings exist in the wave power distribution, which arises from the interference of VLF waveguide modes in the Earth-ionosphere waveguide (Cohen et al., 2012; Cohen & Inan, 2012; Lehtinen & Inan, 2009). This pattern can be observed only in the Southern Hemisphere, which indicates this distribution pattern should evolve and disappear during the propagation from the southern ionosphere to the inner magnetosphere and then to the northern ionosphere.

To check how this wave power distribution changes throughout the propagation from the Southern Hemisphere to the Northern Hemisphere in the inner magnetosphere, we checked the in situ wave observations from two inner magnetospheric spacecraft missions: the Van Allen Probes and the ERG/Arase satellite. Figure 2 shows the distribution of the mean electric field wave power distribution on the transverse plane from the Van Allen Probes'

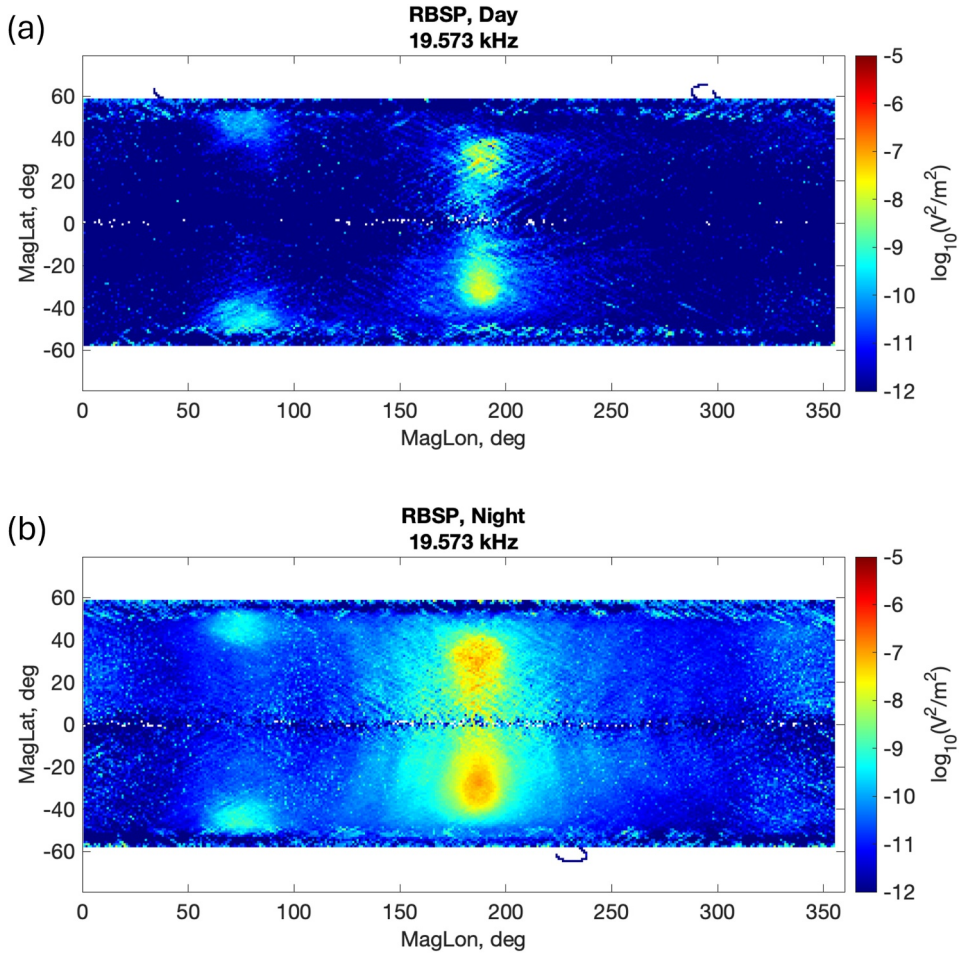

Figure 2. The mean electric field wave power distribution of North West Cape transmitter emission versus geomagnetic latitude and longitude of the footprints at 700 km altitude observed by Van Allen Probes. (a) and (b) are global distributions for day and night sides, respectively.

observation, for the day side (2a) and night side (2b), respectively. The *x* and *y* axes are the geomagnetic longitude and latitude of the satellite's 700 km footprint. The observations with negative local magnetic latitude (the latitude of the satellite in the Geospace) are mapped to the Southern Hemisphere, while those with positive local magnetic latitude are mapped to the Northern Hemisphere. As shown by Figure 2, the concentric rings pattern of the wave power distribution can still be observed by the Van Allen Probes, but becomes less distinct. Based on previous studies (Xia et al., 2023; Zhang et al., 2018), the latitude coverage of the Van Allen Probes for the observation of NWC transmitter signal is mainly confined between −20° and 0°. The wave power distribution in the Northern Hemisphere shown in Figure 2 is derived from a limited number of measurements near the equator at positive local magnetic latitudes. Consequently, the distribution pattern is less smooth than that in the Southern Hemisphere due to the smaller number of data points. And the concentric rings pattern remains observable because the measurements are confined to regions close to the equator. The mean wave power observed by the Van Allen Probes is about one to two orders of magnitude lower than that observed by the DEMETER satellite. This discrepancy is likely due to plasma sheath effects, which create a high-impedance, frequency-dependent barrier between the plasma and the sensor (Hartley et al., 2016, 2017). In summary, the Van Allen Probes can provide observations of the NWC wave power distribution only in the Southern Hemisphere and near the equator region, and whether the concentric ring pattern still exists in the Northern Hemisphere cannot be determined.

Compared to the Van Allen Probes, the ERG/Arase satellite provides better observations to analyze the evolution of the wave power distribution due to its wider local magnetic latitude range. The mean NWC electric field wave power distribution on the transverse plane observed by ERG/Arase is shown in Figure 3. Different from the

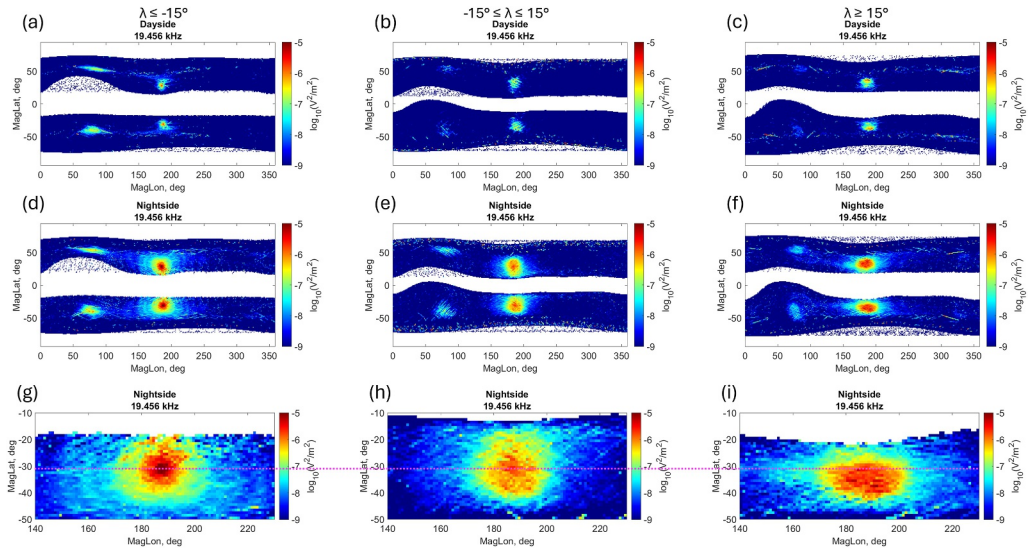

Figure 3. The mean electric field wave power distribution of North West Cape (NWC) transmitter emission versus geomagnetic latitude and longitude of the footprints at 100 km altitude observed by energization and Radiation in Geospace/Arase. The left, middle and right columns are the observations in three local magnetic latitude regions: ≤−15°, −15° to 15° and ≥ 15°, respectively. The first and second rows are the distribution at day and night sides, respectively. The third row is a zoom-in view of the region around the NWC transmitter at night side.

analysis on the Van Allen Probes' observation, we divide the ERG/Arase's observation into three local magnetic region: the Southern Hemisphere region with latitude ≤−15°) (Figures 3a, 3d, and 3g); the near equator region with latitude between −15° and 15° (Figures 3b, 3e, and 3h); and Northern Hemisphere region with latitude ≥ 15° (Figures 3c, 3f, and 3i). The location of the satellite is mapped to both the southern and northern 100 km altitude and plotted in both the Southern and Northern Hemispheres. The first two rows are the day side and night side distributions and the third row is the zoom in of the night side distribution near the location of NWC transmitter in the Southern Hemisphere. These results provide a better view of the evolution of the wave power distribution during propagation. In the Southern Hemisphere region, which is closest to the source region of the transmitter emission, the concentric rings pattern is still observable around the NWC transmitter (Figures 3d and 3g). As the wave propagates to the equator and Northern Hemisphere, the concentric rings pattern disappears (Figures 3e, 3f, 3h, and 3i). Another important evolution is that during the propagation, the shape of the wave power distribution pattern changes from near circular to very elliptical, as well as the center of the pattern moves outward (more southward latitude of footprint, labeled by the magenta dashed line with the latitude of about −30°). All these observed variations of wave power distribution in the inner magnetosphere are consistent with the different distributions in the southern and northern ionosphere observed by DEMETER satellite (Figure 1).

4. Ray Tracing Simulation

To verify the observed evolution of the NWC wave power distribution and better investigate the corresponding propagation process, we performed Ray Tracing simulations to reproduce the wave power distribution in the 3D domain from the topside of the ionosphere to the inner magnetosphere. The ray tracing model used in this simulation is the HOTRAY code (Horne, 1989), the background magnetic field is the IGRF-12 field (Thébault et al., 2015), and the cold plasma density profile used in this study is the typical nighttime profile in Bortnik et al. (2011). Landau damping is also included during the propagation for using a suprathermal electron model (Bortnik et al., 2011) with a moderate Kp value (=2). The initial source rays are launched at the 700 km altitude with geomagnetic longitude range from 100° to 270° and latitude range from −58° to −2°. The source wave power distribution is similar to that observed by the DEMETER satellite (Figure 1). Using the simulated ray paths starting from all the points in the 2D source region, we can calculate the 3D distribution of the NWC wave power in the inner magnetosphere by applying the method used in Xia et al. (2023).

To investigate the best propagation model that reproduce the observed wave power distribution evolution in the inner magnetosphere, we examine 3 propagation modes in the simulation: (a) ducted mode, with wave propagate

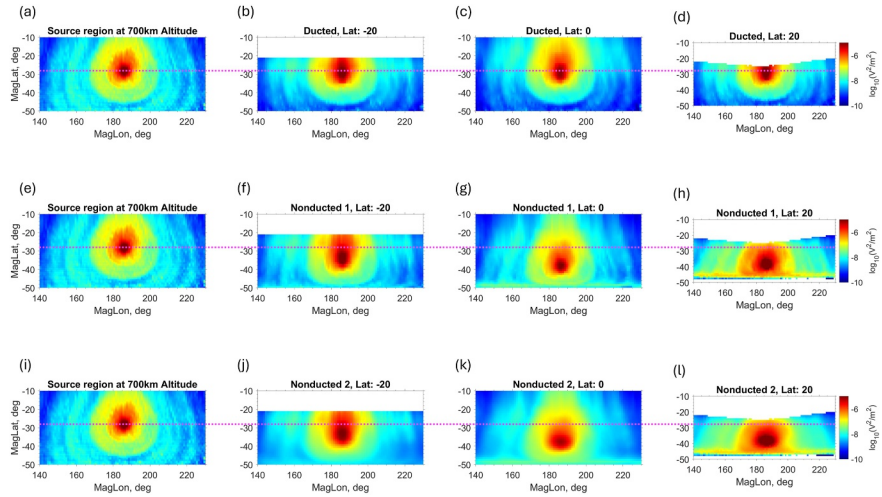

Figure 4. The ray tracing simulated electric field wave power distribution on the transverse plane of North West Cape transmitter. The first column is the source wave power distribution at 700 km altitude observed by DEMETER. The second, third and fourth columns are the simulated distribution at magnetic latitudes of −20°, 0°, and 20°, respectively. The first, second and third rows represent the simulation results for three propagation modes: ducted mode, non-ducted 1 mode, and non-ducted 2 mode, respectively.

along the background magnetic field all the way from the southern ionosphere to the norther ionosphere; (b) non-ducted mode 1, with the initial wave normal angle being exactly vertical outward (the radius outward direction) at the source region; (c) non-ducted mode 2, with initial wave normal spread within a transmission cone that extends to 9° from the vertical outward direction. The transmission cone is nearly vertically outward with a typical angular width of several degrees, according to Snell's law (Zhang et al., 2018). To highlight the difference between the non-ducted 1 and 2 modes, we adopt a transmitter cone width of 9°. The simulated NWC wave power distributions on the transverse plane (geomagnetic longitude-latitude plane of the 700 km southern footprints) at different regions during the propagation are shown in Figure 4. The first column is the initial wave power distribution at the 700 km altitude observed by DEMETER. The second, third and fourth columns are the wave power distribution in the local magnetic latitude of −20°, 0°, 20°, respectively. The first row (Figures 4a–4d) is the result for the ducted propagation mode, in which the wave power distribution remains nearly circular with concentric rings pattern throughout the propagation process. This is pretty reasonable since the wave can only propagate along the magnetic field lines, with no transfer across different magnetic field lines. The second row (Figures 4e–4h) is the result for the non-ducted 1 mode. Different from the ducted mode, as the wave propagates from the Southern Hemisphere to the Northern Hemisphere, the shape of the distribution changes from near circular to oval and the maximum wave power center moves outward. The concentric rings pattern is still clear in the Southern Hemisphere, but becomes indistinct as the wave passes through the equator. This simulated evolution of wave distribution for the non-ducted 1 mode is consistent with the in situ observations. However, compared to the observation, the concentric rings pattern is still clearer in the equator for the ray tracing simulation than the observational result. Thus, we performed the simulation of the non-ducted 2 mode and the result shows better agreement with the observational result: the evolution of the wave power distribution pattern is similar to the non-ducted 1 mode, but the concentric rings pattern becomes more indistinct.

To better understand how different propagation modes result in different wave power distribution, we plot some example ray paths on the meridional plane for the three propagation modes, which are shown in Figure 5. The ray paths correspond to the initial point at 700 km altitude with geomagnetic longitude of 186° and geomagnetic latitudes of −23° (blue), −28° (green) and −33° (red), respectively. Three background magnetic field lines for 1.5, 2, and 2.5 L-shell values are shown by the black dashed lines for reference. For the ducted mode (Figure 5a), the rays propagate exactly along the magnetic field lines and thus the shape of the wave power distribution remains nearly the same on the transverse plane. For the non-ducted 1 mode (Figure 5b), the wave rays propagate outward, which leads to the outward movement of the wave power distribution pattern. In the Northern Hemisphere, the rays tend to concentrate at ∼30°–40° latitude, where the lower hybrid resonance frequency f_{LHR} is maximized. For the non-ducted 2 mode, each source point launches 120 rays with different wave normal angles

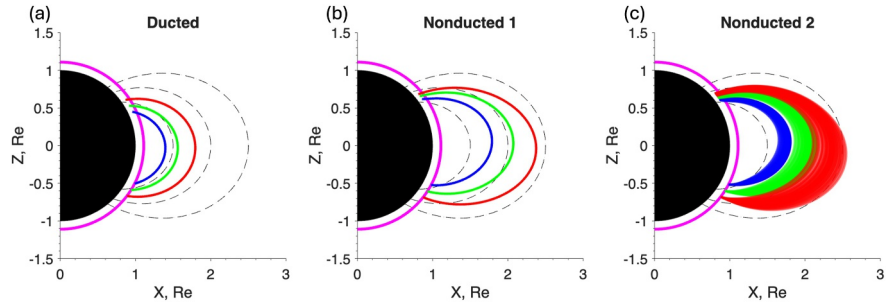

Figure 5. The simulated ray paths on the meridional plane of 186° geomagnetic longitude for rays start from geomagnetic latitudes of −23° (blue), −28° (green) and −33° (red), respectively. (a), (b) and (c) correspond to the simulation for ducted mode, non-ducted 1 mode and non-ducted 2 mode, respectively.

and the ray paths spread in the radial direction and intersect with rays from other source points. Similar overlapping of ray paths also exists in the longitudinal direction (not shown). This intersection of the ray paths from different source points leads to the mixture of wave power from different source regions and diminishes the concentric rings pattern.

Besides the ray-tracing simulations for non-ducted modes with an initially radially outward wave normal angle, we also tested the nonducted case with initial wave normals being parallel to the background magnetic field line, which are suggested by the full wave simulation (Usanova et al., 2022). The results are provided in the Supporting Information S1 in the format similar to Figures 4 and 5. These simulations exhibit significantly inward ray propagation and result in an inward shift of the wave power peak, which is in contrast with observations. Statistically, the non-ducted propagation mode with an initially radially outward wave normal provides better agreement between the simulations and observations for the NWC transmitter emission. In summary of the previous observation and simulation results, we believe that the non-ducted mode, especially with a range of initial wave normal angles, mainly accounts for the evolution of the NWC wave power distribution on the transverse plane during the propagation.

5. Conclusions and Discussions

In this study, the wave power distribution of NWC transmitter emission on the transverse plane and its evolution during the propagation in the magnetosphere are studied based on the in situ observations of DEMETER, Van Allen Probes and ERG/Arase satellites. Ray tracing simulations for 3 different propagation modes of whistler waves are performed to verify and explain the observed wave power distribution of NWC transmitter. The main conclusions are summarized as follows:

1. At the topside of the ionosphere (700 km altitude) in the Southern Hemisphere, the distribution of NWC wave power on the transverse plane observed by DEMETER satellite exhibits concentric rings pattern. At the conjugate point of NWC transmitter in the Northern Hemisphere, the concentric rings pattern disappears and changes from near circle to oval, which indicates a variation of the distribution pattern during the propagation in the inner magnetosphere.
2. As the emission propagates from the ionosphere in the Southern Hemisphere to the equator, and then to the Northern Hemisphere, the center of the distribution pattern moves outward (to higher L-shell) and the distribution becomes more elliptic. The concentric rings pattern is still apparent in the Southern Hemisphere, but becomes indistinct after the wave passes through the equator.
3. Ray tracing simulation results suggest that the non-ducted propagation mode, especially that with spread initial wave normal angles, can account for the evolution of the wave power distribution on the transverse plane, including the outward movement of the distribution pattern and the distinction of the concentric rings pattern.

Our previous study (Xia et al., 2023) investigated the wave power distribution of VLF transmitter signals on the meridional plane, especially the variation of wave amplitude with latitude during propagation in the magnetosphere. Using ray-tracing models, we examined the effects of three main factors relevant to wave power variation: dispersion, geometric, and damping factors. For the NWC transmitter, the wave power variation is primarily controlled by the geometric factor associated with the variation of cross-section area. This study expands the

analysis of VLF transmitter wave power distribution in the magnetosphere from 2D meridional plane to the 3D domain. The observed and modeled wave power distributions on the transverse plane are an important complement to modeling the particle loss due to the VLF transmitter emissions in the inner magnetosphere. The ray tracing simulation explains how the wave power distribution on the transverse plane changes during the propagation and emphasizes the critical role of the non-ducted propagation of the whistler mode waves. However, the whole propagation process in reality cannot be described by one single mode of propagation. The statistical results of observed wave power distribution are attributable to a complex combination of different propagation modes and the contribution of different propagation modes changes in different regions for different transmitters (Němec et al., 2025).

Conflict of Interest

The authors declare no conflicts of interest relevant to this study.

Availability Statement

Science data of the ERG (Arase) satellite were obtained from the ERG Science Center operated by ISAS/JAXA and ISEE/Nagoya University (Miyoshi, Hori, et al., 2018). The data used in this study are level-2 PWE/OFA-SPEC v02.03 data (Kasahara, Kojima, et al., 2018). The ERG/Arase data can be downloaded from https://ergsc.isee.nagoya-u.ac.jp/data/ergsc/satellite/erg/. The Van Allen Probes data can be downloaded from the Space Physics Data Facility https://spdf.gsfc.nasa.gov/pub/data/rbsp/. The DEMETER data can be downloaded from https://cdpp-archive.cnes.fr/. The processed data from the ray tracing simulations, along with the code used to generate Figures 4 and 5 in the article can be downloaded from (Xia, 2026).

Acknowledgments
This work was supported by the AFOSR Grant FA9550-23-1-0568 and the NASA Grants 80NSSC22K1637, 80NSSC24K0174, and 80NSSC25K7749.

References

Albert, J. M., Starks, M. J., Selesnick, R. S., Ling, A. G., O'Malley, S., & Quinn, R. A. (2020). VLF transmitters and lightning-generated whistlers: 2. Diffusion of radiation belt electrons. *Journal of Geophysical Research: Space Physics*, *125*(3), e2019JA027030. https://doi.org/10.1029/2019JA027030

Berthelier, J. J., Godefroy, M., Leblanc, F., Malingre, M., Menvielle, M., Lagoutte, D., et al. (2006). ICE, the electric field experiment on DEMETER. *Planetary and Space Science*, *54*(5), 456–471. https://doi.org/10.1016/j.pss.2005.10.016

Bortnik, J., Chen, L., Li, W., Thorne, R. M., & Horne, R. B. (2011). Modeling the evolution of chorus waves into plasmaspheric hiss. *Journal of Geophysical Research*, *116*(A8). https://doi.org/10.1029/2011JA016499

Budden, K. (1961). *The wave-guide mode theory of wave propagation*. Logos Press. Retrieved from https://books.google.com/books?id=CXREAQAAIAAJ(tex.lccn:62002870)

Cerisier, J. (1973). A theoretical and experimental study of non-ducted VLF waves after propagation through the magnetosphere. *Journal of Atmospheric and Terrestrial Physics*, *35*(1), 77–94. https://doi.org/10.1016/0021-9169(73)90217-1

Chen, L., Xia, Z., Gu, W., & Horne, R. B. (2026). Ground transmitter waves in the magnetosphere and their role in electron scattering. *Journal of Geophysical Research: Space Physics*, *131*, e2026JA035186. https://doi.org/10.1029/2026JA035186

Claudepierre, S. G., Ma, Q., Bortnik, J., O'Brien, T. P., Fennell, J. F., & Blake, J. B. (2020). Empirically estimated electron lifetimes in the earth's radiation belts: Comparison with theory. *Geophysical Research Letters*, *47*(3), e2019GL086056. https://doi.org/10.1029/2019GL086056

Cohen, M. B., & Inan, U. S. (2012). Terrestrial VLF transmitter injection into the magnetosphere. *Journal of Geophysical Research*, *117*(A8), 2012JA017992. https://doi.org/10.1029/2012JA017992

Cohen, M. B., Lehtinen, N. G., & Inan, U. S. (2012). Models of ionospheric VLF absorption of powerful ground based transmitters. *Geophysical Research Letters*, *39*(24), 2012GL054437. https://doi.org/10.1029/2012GL054437

Cunningham, G. S., Botek, E., Pierrard, V., Cully, C., & Ripoll, J.-F. (2020). Observation of high-energy electrons precipitated by NWC transmitter from PROBA-v low-earth orbit satellite. *Geophysical Research Letters*, *47*(16), e2020GL089077. https://doi.org/10.1029/2020GL089077

Gamble, R. J., Rodger, C. J., Clilverd, M. A., Sauvaud, J.-A., Thomson, N. R., Stewart, S. L., et al. (2008). Radiation belt electron precipitation by man-made VLF transmissions. *Journal of Geophysical Research*, *113*(A10). https://doi.org/10.1029/2008JA013369

Graf, K. L., Inan, U. S., Piddyachiy, D., Kulkarni, P., Parrot, M., & Sauvaud, J. A. (2009). DEMETER observations of transmitter-induced precipitation of inner radiation belt electrons. *Journal of Geophysical Research*, *114*(A7). https://doi.org/10.1029/2008JA013949

Gu, W., Chen, L., Xia, Z., An, X., & Horne, R. B. (2020). Alpha transmitter signal reflection and triggered emissions. *Geophysical Research Letters*, *47*(23), e2020GL090165. https://doi.org/10.1029/2020GL090165

Gu, W., Chen, L., Xia, Z., & Horne, R. B. (2021). Direct evidence reveals transmitter signal propagation in the magnetosphere. *Geophysical Research Letters*, *48*(15), e2021GL093987. https://doi.org/10.1029/2021GL093987

Hartley, D. P., Kletzing, C. A., Kurth, W. S., Bounds, S. R., Averkamp, T. F., Hospodarsky, G. B., et al. (2016). Using the cold plasma dispersion relation and whistler mode waves to quantify the antenna sheath impedance of the Van Allen probes EFW instrument. *Journal of Geophysical Research: Space Physics*, *121*(5), 4590–4606. https://doi.org/10.1002/2016JA022501

Hartley, D. P., Kletzing, C. A., Kurth, W. S., Hospodarsky, G. B., Bounds, S. R., Averkamp, T. F., et al. (2017). An improved sheath impedance model for the Van Allen probes EFW instrument: Effects of the spin axis antenna. *Journal of Geophysical Research: Space Physics*, *122*(4), 4420–4429. https://doi.org/10.1002/2016JA023597

Helliwell, R. A. (1966). Whistlers and related ionospheric phenomena. *Geophysical Journal of the Royal Astronomical Society*, *11*(5), 563–564. https://doi.org/10.1111/j.1365-246x.1966.tb03172.x

Horne, R. B. (1989). Path-integrated growth of electrostatic waves: The generation of terrestrial myriametric radiation. *Journal of Geophysical Research*, *94*(A7), 8895–8909. https://doi.org/10.1029/JA094iA07p08895

Inan, U. S., Golkowski, M., Casey, M. K., Moore, R. C., Peter, W., Kulkarni, P., et al. (2007). Subionospheric VLF observations of transmitter-induced precipitation of inner radiation belt electrons. *Geophysical Research Letters*, *34*(2). https://doi.org/10.1029/2006GL028494

Kasahara, Y., Kasaba, Y., Kojima, H., Yagitani, S., Ishisaka, K., Kumamoto, A., et al. (2018). The plasma wave experiment (PWE) on board the arase (ERG) satellite. *Earth Planets and Space*, *70*(1), 86. https://doi.org/10.1186/s40623-018-0842-4

Kasahara, Y., Kojima, H., Matsuda, S., Ozaki, M., Yagitani, S., Shoji, M., et al. (2018). Exploration of energization and radiation in geospace (ERG) plasma wave experiment (PWE) onboard frequency analyzer (OFA) Level-2 power spectrum data. *ERG Science Center, Institute for Space-Earth Environmental Research, Nagoya University*. https://doi.org/10.34515/DATA.ERG-08000

Kletzing, C. A., Kurth, W. S., Acuna, M., MacDowall, R. J., Torbert, R. B., Averkamp, T., et al. (2013). The electric and magnetic field instrument suite and integrated science (EMFISIS) on RBSP. *Space Science Reviews*, *179*(1–4), 127–181. https://doi.org/10.1007/s11214-013-9993-6

Kulkarni, P., Inan, U. S., Bell, T. F., & Bortnik, J. (2008). Precipitation signatures of ground-based VLF transmitters. *Journal of Geophysical Research*, *113*(A7), 2007JA012569. https://doi.org/10.1029/2007JA012569

Lehtinen, N. G., & Inan, U. S. (2009). Full-wave modeling of transionospheric propagation of VLF waves. *Geophysical Research Letters*, *36*(3), 2008GL036535. https://doi.org/10.1029/2008GL036535

Li, X., Ma, Y., Wang, P., Wang, H., Lu, H., Zhang, X., et al. (2012). Study of the north west cape electron belts observed by DEMETER satellite. *Journal of Geophysical Research*, *117*(A4). https://doi.org/10.1029/2011JA017121

Liu, Y., Xiang, Z., Ni, B., Li, X., Zhang, K., Fu, S., et al. (2022). Quasi-trapped electron fluxes induced by NWC transmitter and CRAND: Observations and simulations. *Geophysical Research Letters*, *49*(5), e2021GL097443. https://doi.org/10.1029/2021GL097443

Ma, Q., Gu, W., Claudepierre, S. G., Li, W., Bortnik, J., Hua, M., & Shen, X. (2022). Electron scattering by very-low-frequency and low-frequency waves from ground transmitters in the earth's inner radiation belt and slot region. *Journal of Geophysical Research: Space Physics*, *127*(6), e2022JA030349. https://doi.org/10.1029/2022JA030349

Ma, Q., Mourenas, D., Li, W., Artemyev, A., & Thorne, R. M. (2017). VLF waves from ground-based transmitters observed by the Van Allen probes: Statistical model and effects on plasmaspheric electrons. *Geophysical Research Letters*, *44*(13), 6483–6491. https://doi.org/10.1002/2017GL073885

Matsuda, S., Kasahara, Y., Kojima, H., Kasaba, Y., Yagitani, S., Ozaki, M., et al. (2018). Onboard software of Plasma Wave Experiment aboard Arase: Instrument management and signal processing of Waveform Capture/Onboard Frequency Analyzer. *Earth Planets and Space*, *70*(1), 75. https://doi.org/10.1186/s40623-018-0838-0

Mauk, B. H., Fox, N. J., Kanekal, S. G., Kessel, R. L., Sibeck, D. G., & Ukhorskiy, A. (2013). Science objectives and rationale for the radiation belt storm probes mission. *Space Science Reviews*, *179*(1–4), 3–27. https://doi.org/10.1007/s11214-012-9908-y

Miyoshi, Y., Hori, T., Shoji, M., Teramoto, M., Chang, T. F., Segawa, T., et al. (2018). The ERG science center. *Earth Planets and Space*, *70*(1), 96. https://doi.org/10.1186/s40623-018-0867-8

Miyoshi, Y., Shinohara, I., Takashima, T., Asamura, K., Higashio, N., Mitani, T., et al. (2018). Geospace exploration project ERG. *Earth Planets and Space*, *70*(1), 101. https://doi.org/10.1186/s40623-018-0862-0

Němec, F., Santolík, O., & Albert, J. M. (2025). VLF transmitter signals observed by the cluster spacecraft over a wide range of latitudes. *Journal of Geophysical Research: Space Physics*, *130*(2), e2024JA033621. https://doi.org/10.1029/2024JA033621

Němec, F., Santolík, O., Hospodarsky, G. B., & Kurth, W. S. (2022). Alpha transmitter signals observed by the Van Allen probes: Ducted versus nonducted propagation. *Geophysical Research Letters*, *49*(12), e2022GL098328. https://doi.org/10.1029/2022GL098328

Parrot, M., Benoist, D., Berthelier, J., Błecki, J., Chapuis, Y., Colin, F., et al. (2006). The magnetic field experiment IMSC and its data processing onboard DEMETER: Scientific objectives, description and first results. *Planetary and Space Science*, *54*(5), 441–455. https://doi.org/10.1016/j.pss.2005.10.015

Rodger, C. J., Carson, B. R., Cummer, S. A., Gamble, R. J., Clilverd, M. A., Green, J. C., et al. (2010). Contrasting the efficiency of radiation belt losses caused by ducted and nonducted whistler-mode waves from ground-based transmitters. *Journal of Geophysical Research*, *115*(A12). https://doi.org/10.1029/2010JA015880

Ross, J. P. J., Meredith, N. P., Glauert, S. A., Horne, R. B., & Clilverd, M. A. (2019). Effects of VLF transmitter waves on the inner belt and slot region. *Journal of Geophysical Research: Space Physics*, *124*(7), 5260–5277. https://doi.org/10.1029/2019JA026716

Sauvaud, J.-A., Maggiolo, R., Jacquey, C., Parrot, M., Berthelier, J.-J., Gamble, R. J., & Rodger, C. J. (2008). Radiation belt electron precipitation due to VLF transmitters: Satellite observations. *Geophysical Research Letters*, *35*(9). https://doi.org/10.1029/2008GL033194

Selesnick, R. S., Albert, J. M., & Starks, M. J. (2013). Influence of a ground-based VLF radio transmitter on the inner electron radiation belt. *Journal of Geophysical Research: Space Physics*, *118*(2), 628–635. https://doi.org/10.1002/jgra.50095

Shen, Y., Artemyev, A. V., Ma, Q., Zhang, X., Mourenas, D., Tsai, E., et al. (2022). Inner belt wisp precipitation measured by ELFIN: Regimes of energetic electron scattering by VLF transmitter waves. *Journal of Geophysical Research: Space Physics*, *127*(11), e2022JA030968. https://doi.org/10.1029/2022JA030968

Starks, M. J., Albert, J. M., Ling, A. G., O'Malley, S., & Quinn, R. A. (2020). VLF transmitters and lightning-generated whistlers: 1. Modeling waves from source to space. *Journal of Geophysical Research: Space Physics*, *125*(3), e2019JA027029. https://doi.org/10.1029/2019JA027029

Starks, M. J., Quinn, R. A., Ginet, G. P., Albert, J. M., Sales, G. S., Reinisch, B. W., & Song, P. (2008). Illumination of the plasmasphere by terrestrial very low frequency transmitters: Model validation. *Journal of Geophysical Research*, *113*(A9). https://doi.org/10.1029/2008JA013112

Thébault, E., Finlay, C. C., Beggan, C. D., Alken, P., Aubert, J., Barrois, O., et al. (2015). International geomagnetic reference field: The 12th generation. *Earth Planets and Space*, *67*(1), 79. https://doi.org/10.1186/s40623-015-0228-9

Usanova, M. E., Reid, R. A., Xu, W., Marshall, R. A., Starks, M. J., & Wilson, G. R. (2022). Using VLF transmitter signals at LEO for plasmasphere model validation. *Journal of Geophysical Research: Space Physics*, *127*(4), e2022JA030345. https://doi.org/10.1029/2022JA030345

Xia, Z. (2026). Data for "evolution of nwc transmitter wave power distribution from the topside ionosphere into the inner magnetosphere". *Zenodo*. https://doi.org/10.5281/zenodo.20218847

Xia, Z., Chen, L., Gu, W., Horne, R. B., Miyoshi, Y., Kasahara, Y., et al. (2023). Latitudinal dependence of ground VLF transmitter wave power in the inner magnetosphere. *Frontiers in Astronomy and Space Sciences*, *10*, 1135509. https://doi.org/10.3389/fspas.2023.1135509

Zhang, Z., Chen, L., Li, X., Xia, Z., Heelis, R. A., & Horne, R. B. (2018). Observed propagation route of VLF transmitter signals in the magnetosphere. *Journal of Geophysical Research: Space Physics*, *123*(7), 5528–5537. https://doi.org/10.1029/2018JA025637